

Bidirectional highly-efficient quantum routing in a T-bulge-shaped waveguide

Jia-Hao Zhang(张家豪), Da-Yong He(何大永), Gang-Yin Luo(罗刚银), Bi-Dou Wang(王弼陡), and Jin-Song Huang(黄劲松)

Citation: Chin. Phys. B, 2021, 30 (**3**): 034204. DOI: 10.1088/1674-1056/abd38c
Journal homepage: http://cpb.iphy.ac.cn; http://iopscience.iop.org/cpb

What follows is a list of articles you may be interested in

Design and fabrication of GeAsSeS chalcogenide waveguides with thermal annealing

Limeng Zhang(张李萌), Jinbo Chen(陈锦波), Jierong Gu(顾杰荣), Yixiao Gao(高一骁), Xiang Shen(沈祥), Yimin Chen(陈益敏), and Tiefeng Xu(徐铁峰)
Chin. Phys. B, 2021, 30 (**3**): 034210. DOI: 10.1088/1674-1056/abd757

Far-zone behaviors of scattering-induced statistical properties of partially polarized spatially and spectrally partially coherent electromagnetic pulsed beam

Yan Li(李艳), Ming Gao(高明)†, Hong Lv(吕宏), Li-Guo Wang(王利国), and Shen-He Ren(任神河)
Chin. Phys. B, 2020, 29 (**10**): 104201. DOI: 10.1088/1674-1056/ab9de7

Gain-induced large optical torque in optical twist settings

Genyan Li(李艮艳), Xiao Li(李肖), Lei Zhang(张磊), Jun Chen(陈君)
Chin. Phys. B, 2020, 29 (**8**): 084201. DOI: 10.1088/1674-1056/ab9616

Experimental determination of distributions of soot particle diameter and number density by emission and scattering techniques

Huawei Liu(柳华蔚), Shu Zheng(郑树)
Chin. Phys. B, 2019, 28 (**1**): 014206. DOI: 10.1088/1674-1056/28/1/014206

Single-photon scattering by two separated atoms in a supercavity

Wei Zhu(朱伟), Xiao Xiao(肖骁), Duan-Lu Zhou(周端陆), Peng Zhang(张芃)
Chin. Phys. B, 2016, 25 (**6**): 064203. DOI: 10.1088/1674-1056/25/6/064203

Bidirectional highly-efficient quantum routing in a T-bulge-shaped waveguide*

Jia-Hao Zhang(张家豪)[1,†], Da-Yong He(何大永)[1], Gang-Yin Luo(罗刚银)[1], Bi-Dou Wang(王弼陡)[1], and Jin-Song Huang(黄劲松)[2,‡]

[1] *Engineering Industrialization Research Center, Suzhou Institute of Biomedical Engineering and Technology, Chinese Academy of Sciences, Suzhou* 215011, *China*

[2] *School of Information Engineering, Jiangxi University of Science and Technology, Ganzhou* 341000, *China*

(Received 18 August 2020; revised manuscript received 10 October 2020; accepted manuscript online 15 December 2020)

Quantum routing in a T-bulge-shaped waveguide system coupled with a driven cyclic three-level atom and a two-level atom is investigated theoretically. By employing the discrete-coordinate scattering method, exact expressions of the transport coefficients along three ports of the waveguide channels are derived. Our results show that bidirectional high transfer-rate single-photon routing between two channels can be effectively implemented, with the help of the effective potential generated by two atoms and the external driving. Moreover, multiple band zero-transmission emerges in the scattering spectra, arising from the quantum interferences among photons scattered by the boundary and the bulged resonators. The proposed system may suggest an efficient duplex router with filtering functions.

Keywords: scattering theory, optical waveguide, quantum routing

PACS: 42.50.Ex, 42.79.Gn, 03.67.Lx, 78.67.–n **DOI:** 10.1088/1674-1056/abd38c

1. Introduction

In a quantum network, photons are usually utilized as perfect information carriers to transmit quantum information over long distances,[1] and thus, it is of great importance to tailor and enhance the light–matter interactions to route efficiently these photons in different quantum channels. In the past decades, the strong field–matter interactions have be achieved by waveguide quantum electrodynamics (QED) systems,[2–7] and many interesting transport properties such as optical nonreciprocity and directional light amplification have still been exploited experimentally.[8–12] With the ideal platform, quantum routing of single photons is also investigated, where waveguide is utilized as the quantum channel, and the photon signal transport is controlled effectively via the strong light–matter interactions. Accordingly, numerous theoretical[13–26] and experimental[27–30] investigations on the quantum routing of single photons have been demonstrated in many waveguide-QED systems. For example, Zhou *et al.* examined the single-photon quantum routing properties in an X-shaped coupled-resonator waveguide (CRW), and showed that efficient routing can be implemented between two quantum channels with the help of a classical field.[13,14] By using the interferences of photons with the phase differences, a router with multi-output ports has also been investigated by Yan *et al.*[15]

However, in a multichannel quantum network, there exists a confine of low routing rate (no excess of 0.5) of single photons transmitted between different channels in many proposed routers, owing to extended assignments for the increasing ports. This could limit their potential applications, since the desired high routing capability of redirecting the incident photons into another channel is very essential for the efficient distributions of transmission signals. To enhance the inter-channel transfer rate of routed photons, a T-shaped or an extended T-bulge-shaped waveguide[16,17] is proposed to achieve it via the radiation field modification from the boundary effect of the semi-infinite CRW, and an unidirectional high probability transfer only from the semi-infinite channel to the infinite one is realized. Thus, it is of considerable interest to design a high-efficiency router with bidirectional high transfer-rate routing.

Motivated by these considerations, we extend the previous single-atom coupled scheme and propose a two-atom coupled one to effectively perform bidirectional high-efficiency quantum routing of single photons in a T-bulge-shaped waveguide system, in which a three-level atom and an additional two-level atom are coupled. By applying the discrete-coordinate scattering approach, the single-photon scattering amplitudes into three ports of the waveguide network are obtained analytically. Then, we examine how to efficiently control the quantum routing of the single photons by tuning the atom-resonator coupling strengths and the driving field. In

*Project supported by the National Key Research and Development Program of China (Grant No. 2017YFC0110403) and the Scientific Research Foundation of the Jiangxi Provincial Education Department, China (Grant No. GJJ180424).

†Corresponding author. E-mail: zjhhank2016@163.com

‡Corresponding author. E-mail: jshuangjs@126.com

© 2021 Chinese Physical Society and IOP Publishing Ltd

contrast to the previous schemes[11,12] with a unidirectional high transfer-rate routing from the semi-infinite channel to the infinite channel, bidirectional highly-efficient routing between two channels can be achieved via the effective potential from the additional atom. In addition, compared to the T-shaped waveguide system with the bare boundary, multiple band zero-transmission with filtering function is exhibited in the scattering spectra, due to the multiple quantum interferences of these photons located in the boundary and the bulged resonators in the T-bulge-shaped waveguide system. Therefore, the proposed system can be utilized as a multi-function router.

2. Theoretical method

The schematic diagram of a coupled T-bulge-shaped waveguide is shown in Fig. 1. Two cross optical channels are constructed by one infinite CRW-a and another semi-infinite CRW-b with $N-1$ bulged resonators below the cross resonator. These resonator modes of two CRWs are described by the creation operators $a^{\dagger}_{j_a}$ and $b^{\dagger}_{j_b}$, respectively, with the subscripts $j_a = -\infty, \ldots, +\infty$, and $j_b = 1, \ldots, +\infty$. A Δ-type three-level atom, placed at the crosspoint $(j_a = 0, j_b = N)$ of two CRWs, is characterized by a ground state $|g\rangle$ and two excited states $|e\rangle$ and $|f\rangle$. The cavity modes b_N and a_0 in the cross resonator couple the transitions $|g\rangle \leftrightarrow |f\rangle$ and $|g\rangle \leftrightarrow |e\rangle$ with the coupling strengths g_b and g_a, respectively. The transition $|e\rangle \leftrightarrow |f\rangle$ is resonantly driven by a classical field with frequency ν and Rabi frequency Ω. Here, the transition between the ground state and the intermediate state is unforbidden for these cyclic structures, which can exist in artificial symmetry-broken systems.[31,32] Another two-level atom characterized by ground states $|g_2\rangle$ and excited states $|e_2\rangle$ can be located at two possible locations such as the right of CRW-a or the above of CRW-b. We first investigate the case that the two-level atom is placed at $j_a = p$ of the CRW-a, and also coupled to the CRW-a with the coupling constant g_p.

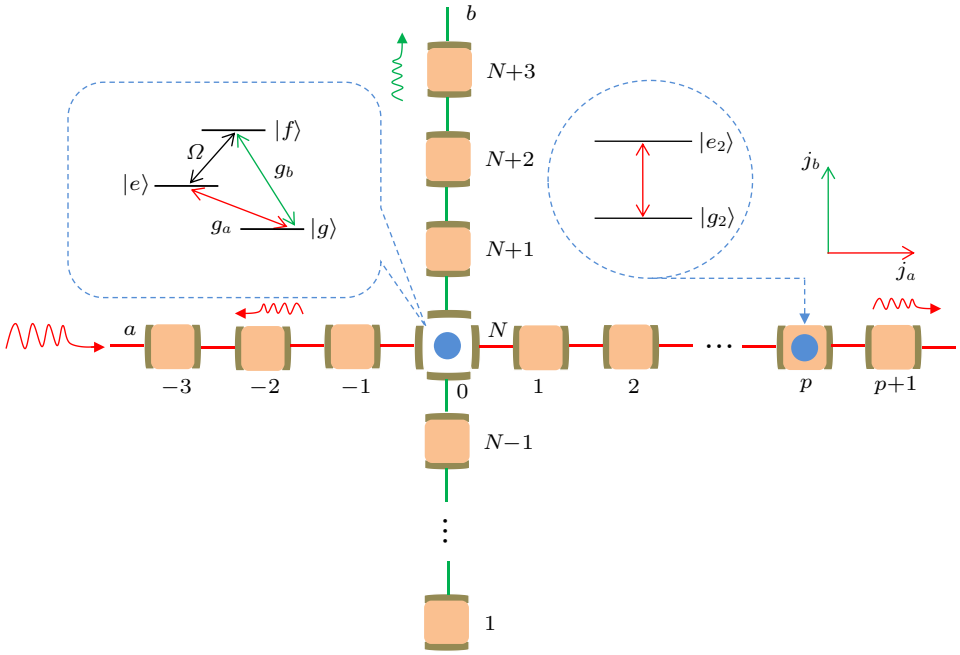


Fig. 1. Schematic view of routing single photons in two channels formed by one infinite CRW and another semi-infinite CRW with $N-1$ bulged resonators below the cross resonator. A three-level system, located at the crosspoint $(j_a = 0,\ j_b = N)$, is resonantly driven by a classical field Ω. Another two-level atom is located at $j_a = p$. A single photon incoming from the left side of CRW-a is reflected, transmitted, or transferred to CRW-b.

When a photon is incident from one cavity of the CRW-a, it propagates with the transmission probability T_a or is reflected by the atoms along the channel-a with the reflection probability R_a, and it is also routed into CRW-b with the transfer rate T_b, with the help of a driving. The total Hamiltonian of the composite system consists of three parts

$$H = H_{\rm w} + H_a + H_{\rm int}, \tag{1}$$

where $H_{\rm w}$ describes the photon propagation in the waveguide, H_a denotes the Hamiltonian of the three-level and two-level atoms, and $H_{\rm int}$ describes the interactions among the resonator modes, the classical driving and two atoms. The three terms can be expressed as ($\hbar = 1$ throughout)

$$\begin{aligned} H_{\rm w} &= \sum_{j_a}[\omega_a a^{\dagger}_{j_a} a_{j_a} - \xi_a(a^{\dagger}_{j_a} a_{j_a+1} + a^{\dagger}_{j_a+1} a_{j_a})] \\ &\quad + \sum_{j_b}[\omega_b b^{\dagger}_{j_b} b_{j_b} - \xi_b(b^{\dagger}_{j_b} b_{j_b+1} + b^{\dagger}_{j_b+1} b_{j_b})], \\ H_a &= \omega_{e_1}|e\rangle\langle e| + \omega_f|f\rangle\langle f| + \omega_{e_2}|e_2\rangle\langle e_2|, \\ H_{\rm int} &= g_a|e\rangle\langle g|a_0 + g_b|f\rangle\langle g|b_N + g_p|e_2\rangle\langle g_2|a_p \\ &\quad + \Omega\,{\rm e}^{-{\rm i}\nu t}|f\rangle\langle e| + {\rm H.c.}, \end{aligned} \tag{2}$$

where we have set the energy levels of the atomic ground states as the energy references. For simplicity, we have supposed that all resonators in the CRW-a (b) have the same

frequency ω_a (ω_b) and the hopping coefficient ξ_a (ξ_b) between any two nearest-neighbor resonators in the CRW-a (b) is equal. $\omega_{e_1(f,e_2)}$ represents the frequency of atomic state $|e(f,e_2)\rangle$. $a^\dagger_{j_a}$ ($b^\dagger_{j_b}$) is the creation operator of photon at site $j_a(j_b)$ of the CRW-a (b). The Hamiltonian of the coupled-resonator waveguide in Eq. (2) describes a typical tight-binding boson model,[13,14] which presents the dispersion relations $E_k^{[a]} = \omega_a - 2\xi_a\cos(k_a\varsigma)$ and $E_k^{[b]} = \omega_b - 2\xi_b\cos(k_b\varsigma)$, with wavenumbers k_a and k_b. Here, the lattice constant ς is assumed to be unity.

By performing a time-dependent unitary transformation $H_{\rm eff} = U^\dagger H U - {\rm i}U^\dagger\partial U/\partial t$ with the operator $U = {\rm e}^{-{\rm i}\nu t|e\rangle\langle e|}$, one gets the effective Hamiltonian under the rotating framework

$$\begin{aligned} H_a &= \omega_e|e\rangle\langle e| + \omega_f|f\rangle\langle f| + \omega_{e_2}|e_2\rangle\langle e_2|, \\ H_{\rm int} &= g_a|e\rangle\langle g|a_0 + g_b|f\rangle\langle g|b_N + g_p|e_2\rangle\langle g_2|a_p \\ &\quad + \Omega|f\rangle\langle e| + {\rm H.c.}, \end{aligned} \tag{3}$$

where $\omega_e = \omega_{e_1} - \nu$ is the detuning of the atomic state $|e\rangle$ from the driving. The Hamiltonian of the waveguide part remains the same.

Since the total number of excitations is conserved in this hybrid system, the eigenstate of Hamiltonian (1) is given by

$$|\psi\rangle = \sum_{j_a}\alpha(j_a)a^\dagger_{j_a}|\emptyset_a,\emptyset_b,g,g_2\rangle + \sum_{j_b}\beta(j_b)b^\dagger_{j_b}|\emptyset_a,\emptyset_b,g,g_2\rangle + c_e|\emptyset_a,\emptyset_b,e,g_2\rangle + c_f|\emptyset_a,\emptyset_b,f,g_2\rangle + c_2|\emptyset_a,\emptyset_b,g,e_2\rangle, \tag{4}$$

where $|\emptyset_a,\emptyset_b\rangle$ describes the waveguide vacuum state. $\alpha(j_a)$ and $\beta(j_b)$ denote the probability amplitudes of photons in the j_a-th cavity of CRW-a and j_b-th cavity of CRW-b, respectively. c_e (c_f, c_2) is the excitation amplitude of the atomic state $|e\rangle$ ($|f\rangle$, $|e_2\rangle$).

From the eigen-equation $H|\psi\rangle = E_k|\psi\rangle$, we get

$$\begin{aligned} &(E_k-\omega_{e_2})c_2 = g_p\alpha(p), \quad (E_k-\omega_e)c_e = \Omega c_f + g_a\alpha(0), \quad (E_k-\omega_f)c_f = \Omega^* c_e + g_b\beta(N), \\ &(E_k-\omega_a)\alpha(j_a) = -\xi_a[\alpha(j_a-1)+\alpha(j_a+1)] + \delta_{j_a0}g_a c_e + \delta_{j_ap}g_p c_2, \\ &(E_k-\omega_b)\beta(j_b) = -\xi_b[\beta(j_b-1)+\beta(j_b+1)] + \delta_{j_bN}g_b c_f, \end{aligned} \tag{5}$$

where the dispersion relation $E_k = E_k^{[a]} = E_k^{[b]}$ is satisfied. Removing these atomic amplitudes c_e and c_f, we obtain the scattering equation

$$\begin{aligned} (E_k-\omega_a)\alpha(j_a) &= -\xi_a[\alpha(j_a-1)+\alpha(j_a+1)] + \delta_{j_a0}[V_a\alpha(0)+G\beta(N)] + \delta_{j_ap}V_p\alpha(p), \\ (E_k-\omega_b)\beta(j_b) &= -\xi_b[\beta(j_b-1)+\beta(j_b+1)] + \delta_{j_bN}[V_b\beta(N)+G^*\alpha(0)]. \end{aligned} \tag{6}$$

The coupling between the three-level atom and CRWs yields the energy-dependent effective potentials with strengths

$$\begin{aligned} V_a(E_k) &= \frac{g_a^2\Delta_f}{\Delta_e\Delta_f - |\Omega|^2}, \\ V_b(E_k) &= \frac{g_b^2\Delta_e}{\Delta_e\Delta_f - |\Omega|^2}, \\ V_p &= \frac{g_p^2}{\Delta_{e_2}}, \end{aligned} \tag{7}$$

and the dispersive coupling strength between two CRWs

$$G(E_k) = \frac{\Omega g_a g_b}{\Delta_e\Delta_f - |\Omega|^2}. \tag{8}$$

Here, $\Delta_e = E_k - \omega_e$, $\Delta_f = E_k - \omega_f$, $\Delta_{e_2} = E_k - \omega_{e_2}$. The effective potentials and the dispersive coupling strength G play important roles for the routing properties of single photons.

3. Quantum routing properties of single photons

Considering the coupled T-bulge-shaped waveguide system as a two-channel quantum router, we thus focus on routing rate of single photons from one CRW to the other. As the structural symmetry is break by the boundary of the CRW-b, we examine two cases of incident waves incoming from both CRWs, respectively.

3.1. Single photons incident from the left side of CRW-a

We consider the first case of a single photon incoming from the left of CRW-a. There are two possible locations for the two-level atom, *e.g.*, in the right of CRW-a or in the above of CRW-b. We first discuss the former, as shown in Fig. 1. The corresponding wave functions have the solutions

$$\alpha(j_a) = \begin{cases} {\rm e}^{{\rm i}j_ak_a} + r_a{\rm e}^{-{\rm i}j_ak_a}, & j_a < 0, \\ t_1{\rm e}^{{\rm i}j_ak_a} + r_1{\rm e}^{-{\rm i}j_ak_a}, & 0 < j_a < p, \\ t_a{\rm e}^{{\rm i}j_ak_a}, & j_a > p, \end{cases} \tag{9}$$

$$\beta(j_b) = \begin{cases} A\sin(Nk_b), & j_b = 1,2,\ldots,N, \\ t_b{\rm e}^{{\rm i}j_bk_b}, & j_b > N, \end{cases} \tag{10}$$

where r_1 and t_1 represent reflection and transmission amplitudes between the 0-th and p-th resonators in CRW-a, respectively. r_a, t_a, and t_b are reflection, transmission in CRW-a, and transfer in CRW-b, respectively. A is an amplitude constant at the boundary cavity $j_b \le N$.

Substituting Eqs. (9) and (10) into Eq. (6), after some algebra, we obtain the scattering amplitudes

$$r_a = \frac{2i\xi_a \sin k_a(\xi_b F - \xi_b e^{-ik_b} - V_b)}{C_p(\xi_b F - \xi_b e^{-ik_b} - V_b) - |G|^2} - 1, \quad t_a = \frac{-4\xi_a^2 \sin^2 k_a(\xi_b F - \xi_b e^{-ik_b} - V_b) e^{-2ipk_a}}{[(2i\xi_a \sin k_a - V_p) e^{-2ipk_a} + V_p][C_p(\xi_b F - \xi_b e^{-ik_b} - V_b) - |G|^2]},$$
$$t_b = \frac{2i\xi_a \sin k_a G e^{-iNk_b}}{C_p(\xi_b F - \xi_b e^{-ik_b} - V_b) - |G|^2}, \quad C_p = \frac{2i\xi_a \sin k_a(2i\xi_a \sin k_a - V_p) e^{-2ipk_a}}{(2i\xi_a \sin k_a - V_p) e^{-2ipk_a} + V_p} - V_a, \quad F = \frac{\sin[(N-1)k_b]}{\sin(Nk_b)}. \tag{11}$$

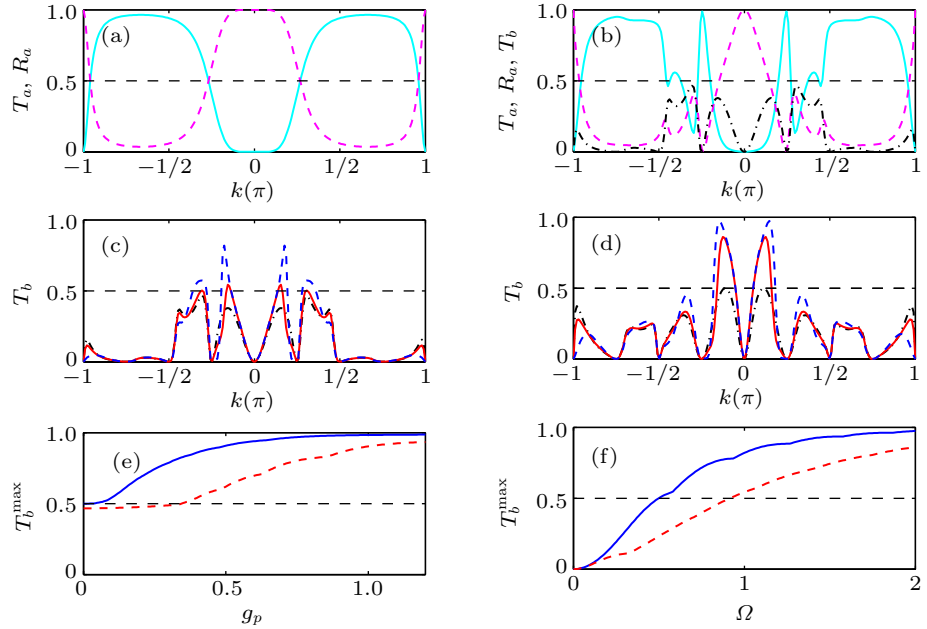


Fig. 2. (a) Transmission T_a (cyan solid line) and reflection R_a (pink dashed line) as a function of the momentum k for $\Omega = 0$ and $g_n = 0$. (b) Transmission T_a (cyan solid line), reflection R_a (pink dashed line), transfer T_b (black dash dotted line) for $\Omega = 1$ and $g_n = 0$. Transfer T_b for different g_p: black dash dotted line for $g_p = 0$, red solid line for $g_p = 0.4$, and blue dashed line for $g_p = 0.8$, in (c) $\Omega = 1.0$, and (d) $\Omega = 2.0$, respectively. (e) Maximum transfer $T_b^{\max}$ as a function of g_p (red dashed line for $\Omega = 1$ and blue solid line for $\Omega = 2$). (f) Maximum transfer $T_b^{\max}$ as a function of Ω (red dashed line for $g_p = 0.4$, and blue solid line for $g_p = 0.8$). The other parameters are taken as $g_a = g_b = 1.0$, $\omega_0 - \omega_e = 2$, $\omega_0 - \omega_f = 1.6$, $\omega_0 - \omega_{e2} = 2$, $\xi_a = \xi_b = \xi_0 = 1$, $p = 4$, and $N = 4$, respectively.

In the system with three ports, scattering properties are engineered by the transmission $T_a = |t_a|^2$, reflection $R_a = |r_a|^2$, and transfer $T_b = |t_b|^2$. For simplicity, we assume $\omega_a = \omega_b = \omega_0$, $\omega_e = \omega_{e2}$, $\xi_a = \xi_b = \xi_0$, and $k_a = k_b = k$ in our discussion. In our numerical calculations, these parameters are taken as $\omega_0 - \omega_f = 1.6$, $\omega_0 - \omega_e = 2$, $\omega_0 - \omega_{e2} = 2$, $g_a = g_b = 1$, and $\xi_0 = 1$, and all the parameters are in units of the hopping coefficient ξ_0. It is a reasonable selection, since the adopted parameters are close to the same order of magnitude in a circuit QED experimental system,[33,34] and the waveguide can be constructed by the superconducting transmission-line resonators.

As a contrast, we first research the single-atom case with $g_p = 0$, in which the scattering coefficients in Eq. (11) are reduced to the forms in Ref. [17], where only a driven three-level atom is used to scatter the single photon. If the classical drive is turned off, it is easy to see from Eq. (11) that CRW-b is not coupled to CRW-a, and the incoming photon cannot be routed into another channel completely. In this case, the cyclic three-level atom degenerate to a two-level atom with a single excitation path, and serves as a perfect mirror to completely reflect the input photon at the resonance point, as shown in Fig. 2(a). When the classical field is open, another output channel (CRW-b) is connected, and the conservation relation of the photon flow becomes $|t_a|^2 + |r_a|^2 + |t_b|^2 = 1$. With the help of the classical drive, the single photons are redirected from CRW-a into CRW-b, and the transfer T_b of no more than 0.5 is presented in Fig. 2(b).

When another atom is utilized to be located in the p-th resonator of the CRW-a, there are some different features to be presented. When $g_p = 0$, T_b with no more than 0.5 (black dash dotted curves) is presented in Figs. 2(b)–2(d), even for the strong driving. Whereas increasing g_p, high transfer rate $T_b > 0.5$ occurs, and a transfer $T_b \approx 1$ (blue dashed curves) emerges for $g_p = 0.8$ and $\Omega = 1.0$, as shown in Fig. 2(d). Further, figures 2(e) and 2(f) shows the effects of the coupling strength and driving on the maximum transfer rate $T_b^{\max}$ in the scattering spectra. As seen, the maximum transfer rates also increase with the increasing coupling strength and driving. This scenario may result from the effect of a quantum supercavity[7] generated by two atoms located in 0-th and p-th cavities in CRW-a, where the effective potentials related to the couplings are formed. When the incident photon collides with a repulsive potential, the transmission is blocked, which has been demonstrated by Zhou.[7] Thus, when a single photon comes into the supercavity, it can go through it, or is localized in the area due to the reflection from the effective potential V_p. The localized photon can also be routed into CRW-b with the assistance of the drive, and thus the transfer rate into channel-b is enhanced. Therefore, increasing the coupling g_p and the

drive will give rise to a higher transfer rate into CRW-b, due to their joint effects.

What is more interesting, we find that there exists $2N$ zero-value transmission in the scattering spectra for the N bulged resonators, except the point of $k=0$ ($\upsilon_g = 2\xi_a \sin k = 0$) for no incident wave, which may result from the multiple quantum interferences among the standing waves scattered by the boundary and the bulged resonators. This may provide a potential application as a multi-wavelength filter. With such a device, the desired wavelengths in the output port are selected to drop, which can be used in designing multi-wavelength selectors, multiplexers, and other optical devices.

As a contrast, we also examine another case in which the two-level atom is placed at $j_b = m$ of the CRW-b. In the case, the atom interacts with m-th cavity mode in CRW-b, with the interaction Hamiltonian $H_{\rm int} = g_a|e\rangle\langle g|a_0 + g_b|f\rangle\langle g|b_N + g_m|e_2\rangle\langle g_2|b_m + \Omega|e\rangle\langle f| + \text{H.c.}$ Similar to the above process, after some algebra, we get the scattering amplitudes

$$
\begin{aligned}
r_a &= \frac{2\mathrm{i}\xi_a \sin k_a C_m}{(2\mathrm{i}\xi_a \sin k_a - V_a)C_m - |G|^2} - 1, \quad t_a = \frac{2\mathrm{i}\xi_a \sin k_a C_m}{(2\mathrm{i}\xi_a \sin k_a - V_a)C_m - |G|^2}, \\
t_b &= \frac{-4\xi_a\xi_b \sin k_a \sin k_b G^* \,\mathrm{e}^{-\mathrm{i}(2m-N)k_b}}{[(2\mathrm{i}\xi_b \sin k_b - V_m)\,\mathrm{e}^{-\mathrm{i}(2m-N)k_b} + V_m \,\mathrm{e}^{-\mathrm{i}Nk_b}][(2\mathrm{i}\xi_a \sin k_a - V_a)C_m - |G|^2]}, \\
C_m &= \frac{\sin[(N-1)k_b]}{\sin(Nk_b)}\xi_b - \frac{\xi_b(2\mathrm{i}\xi_b \sin k_b - V_m)\,\mathrm{e}^{-\mathrm{i}(2m-N+1)k_b} + \xi_b V_m \,\mathrm{e}^{-\mathrm{i}(N-1)k_b}}{(2\mathrm{i}\xi_b \sin k_b - V_m)\,\mathrm{e}^{-\mathrm{i}(2m-N)k_b} + V_m \,\mathrm{e}^{-\mathrm{i}Nk_b}} - V_b,
\end{aligned} \tag{12}
$$

where $V_m = g_m^2/\Delta_{e_2}$.

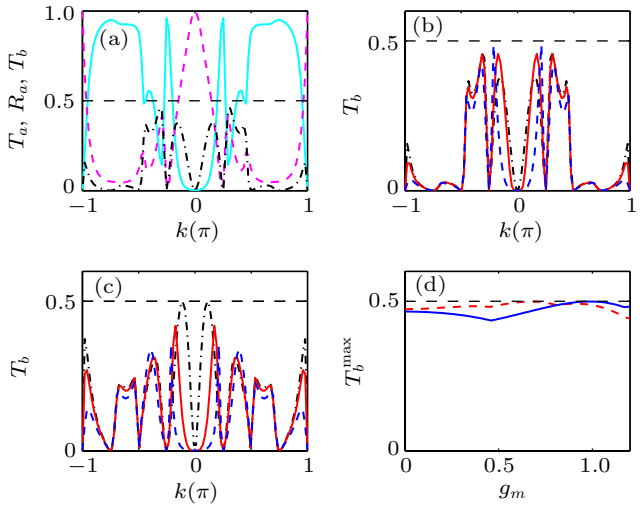


Fig. 3. (a) Transmission T_a (cyan solid line), reflection R_a (pink dashed line), and transfer T_b (black dash dotted line) as a function of the momentum k. (b) Transfer T_b for different g_m: blue dashed line for $g_m = 0$, red solid line for $g_m = 0.4$, and cyan dotted line for $g_m = 0.8$, with (b) $\Omega = 1$, and (c) $\Omega = 2$, respectively. (d) Maximum transfer $T_b^{\max}$ as a function of g_m (red dashed line for $\Omega = 1$ and blue solid line for $\Omega = 2$). Here $m = 4$, and the other parameters are the same as those in Fig. 2.

Similarly, owing to the locality of the quantum supercavity formed in channel-b, the photons transmitted into the supercavity are trapped and reflowed under the effects of the effective potentials, and returned to channel-a for the strong reflection. Since the two ongoing paths along the right side of channel-a and channel-b are reciprocal, the transport probabilities in two paths cannot exceed 0.5, as demonstrated in Refs. [16,17]. Moreover, some photons may be redirected into channel-a, and thus, the transfer rate T_b is less than 0.5, as shown in Figs. 3(a)–3(c). The maximum transfer rate $T_b^{\max}$ with no excess of 0.5 is also exhibited in Fig. 3(d) for the different coupling g_m.

3.2. Single photons incident from the upward side of the CRW-b

We then discuss the case of a single photon incoming from the CRW-b, in which the two-level atom is located in $j_a = n$ of the CRW-a.

Using the similar process of the calculation in case 1, we get the scattering amplitudes

$$
\begin{aligned}
t_a^{\rm l} &= \frac{2\mathrm{i}G^*\xi_b \sin k_b \,\mathrm{e}^{-\mathrm{i}Nk_b}}{C_n(\xi_b F - \xi_b \,\mathrm{e}^{-\mathrm{i}k_b} - \tilde{V}_b) - |G|^2}, \quad t_a^{\rm r} = \frac{-4G^*\xi_a\xi_b \sin k_a \sin k_b \,\mathrm{e}^{-2\mathrm{i}nk_a}\,\mathrm{e}^{-\mathrm{i}Nk_b}}{[(2\mathrm{i}\xi_a \sin k_a - V_n)\,\mathrm{e}^{-2\mathrm{i}nk_a} + V_n][C_n(\xi_b F - \xi_b \,\mathrm{e}^{-\mathrm{i}k_b} - \tilde{V}_b) - |G|^2]}, \\
r_b &= \frac{2\mathrm{i}C_n\xi_b \sin k_b \,\mathrm{e}^{-2\mathrm{i}Nk_b}}{C_n(\xi_b F - \xi_b \,\mathrm{e}^{-\mathrm{i}k_b} - \tilde{V}_b) - |G|^2} - \mathrm{e}^{-2\mathrm{i}Nk_b}, \quad C_n = \frac{2\mathrm{i}\xi_a \sin k_a (2\mathrm{i}\xi_a \sin k_a - V_n)\,\mathrm{e}^{-2\mathrm{i}nk_a}}{(2\mathrm{i}\xi_a \sin k_a - V_n)\,\mathrm{e}^{-2\mathrm{i}nk_a} + V_n} - \tilde{V}_a.
\end{aligned} \tag{13}
$$

Here, r_b, $t_a^{\rm l}$, and $t_a^{\rm r}$ are the reflection amplitude in CRW-b, left and right transmission amplitudes in CRW-a, respectively. Notice that the coupling channels for g_a and g_b are exchanged to retain energy transition with the help of the driving, thus the effective potentials and the dispersive coupling strength between two CRWs are given respectively as

$$
\begin{aligned}
\tilde{V}_a &= \frac{g_a^2\Delta_e}{\Delta_e\Delta_f - |\Omega|^2}, \quad \tilde{V}_b = \frac{g_b^2\Delta_f}{\Delta_e\Delta_f - |\Omega|^2}, \\
V_n &= \frac{g_n^2}{\Delta_{e_2}}, \quad G = \frac{\Omega g_a g_b}{\Delta_e\Delta_f - |\Omega|^2}.
\end{aligned} \tag{14}
$$

In this three-port system, scattering properties are governed by the reflection $R_b = |r_b|^2$, and transfers $T_a^{\rm l} = |t_a^{\rm l}|^2$ and $T_a^{\rm r} = |t_a^{\rm r}|^2$. For the single-atom case ($g_n = 0$), the classical field drives single photons from CRW-b into CRW-a, and the equal transfers $T_a^{\rm l} = T_a^{\rm r}$ overlap each other, due to the symmetrical transmission in both sides of channel-a. While for $g_n \neq 0$, the transfers $T_a^{\rm l}$ and $T_a^{\rm r}$ in CRW-a separate by the scattering of the additional two-level atom, as shown in Fig. 4(a) with $g_n = 0.8$.

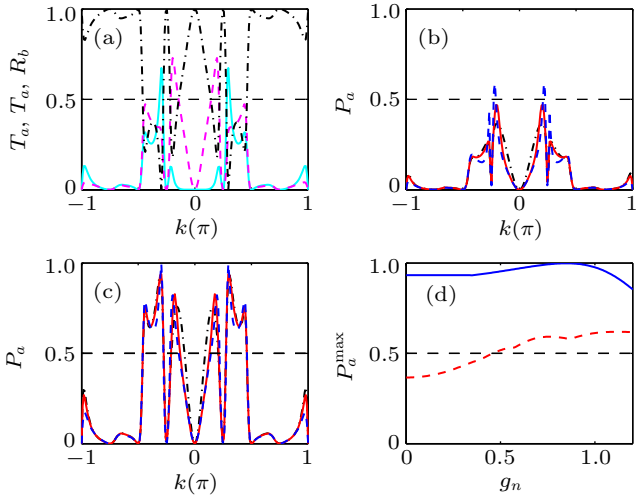


Fig. 4. (a) Reflection R_b (black dash dotted line), transfers $T_a^{\rm r}$ (cyan solid line) and $T_a^{\rm l}$ (pink dashed line) as a function of the momentum k for $\Omega = 1$ and $g_n = 0.8$. Transfer rate P_a for different g_n: blue dashed line for $g_n = 0$, red solid line for $g_n = 0.4$, and cyan dotted line for $g_n = 0.8$, with (b) $\Omega = 0.5$, and (c) $\Omega = 1$, respectively. (d) Maximum transfer $P_a^{\max}$ as a function of g_n (red dashed line for $\Omega = 0.5$ and blue solid line for $\Omega = 1$). Here $n = 3$, and the other parameters are the same as those in Fig. 2.

To examine the dependence of the transfer rate from channel-b to channel-a on the coupling g_n, figures 4(b)–4(c) display the transfer P_a against the coupling for two drives $\Omega = 0.4, 0.8$, respectively. Here, $P_a = T_a + R_a$ is used to denote the total probability of the incident single photons appearing in CRW-a. When $g_n = 0$ and a modern driving $\Omega = 0.5$, $P_a < 0.5$ (blue solid curves) is presented in Fig. 4(b), whereas $P_a > 0.5$ is shown for a large driving $\Omega = 1$ in Fig. 4(c). Moreover, it can be found in Figs. 4(b)–4(c) that a transfer rate approaching unity also emerges when increasing of the coupling strength g_n, and figure 4(d) further indicates the high transfer rate of the maximum $P_a^{\max}$ in the scattering spectra can be controlled under the joint effects of the coupling strength and the driving. This reveals that a bidirectional highly-efficient quantum routing can be implemented in the waveguide system with an additional atom.

In addition, $2N$ zero-value asymmetrical transmission for $T_a^{\rm l}$ and $T_a^{\rm r}$ in two ports of channel-a is also exhibited, as shown in Fig. 4(a), which means that the proposed device is a multi-function router with the multi-band filtering.

4. Discussion and conclusion

Notice that the dissipations are not taken into account in the above discussions. In a real experiment, the composite system inevitably suffers dissipations like the atomic excited-state relaxation and cavity field leakage during propagation. As an example, the exact forms of the scattering amplitudes with dissipations in Case 1 are given in Appendix A, and it is easy to check that the mathematic forms can be reduced to these results in Eq. (11) by assuming zero dissipations.

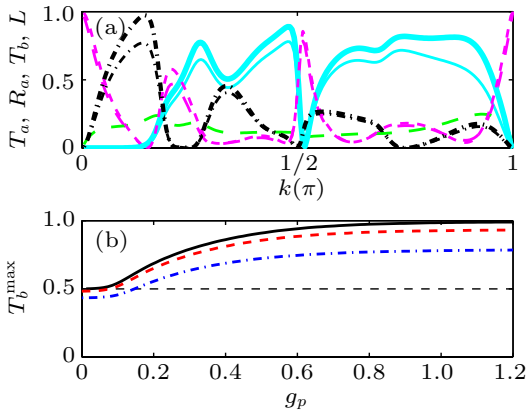


Fig. 5. (a) Transmission T_a (cyan solid line), reflection R_a (pink dashed line), transfer T_b (black dash dotted line), and loss L (green dash line below 0.5) at $\Omega = 2$ and $g_p = 0.8$ for zero dissipations (thick curves) and $\gamma_a = \gamma_b = 0.02$ (thin curves). (b) Maximum transfer rate $P_b^{\max}$ for different coupling g_p at $\Omega = 2$ (black solid line for zero dissipations, red dashed line for $\gamma_a = \gamma_b = 0.005$, and blue dash dotted line for $\gamma_a = \gamma_b = 0.02$). $\gamma_e = \gamma_f = \gamma_{e_2} = 0.001$. The other parameters are the same as those in Fig. 2.

For the forward photon with a group velocity $\upsilon_g = 2\xi \sin k$, figure 5 shows the influences of the cavity decays and atomic relaxations on the routing properties. In the calculation, the choices of the dissipative parameters are based on the experimental results in Refs. [34,35]. The ratio of resonator decay $\gamma_{a(b)}$ to its coupling strength $g_{a(b)}$ is adopted to be around 0.005 for the general superconducting coplanar resonator, or more small for a high-Q cavity. Comparing the spectral probabilities of the reflection R_a, transmission T_a, and transfer T_b, we can find that all of these scattering probabilities are reduced (see Fig. 5(a)) owing to the outside leakage. The loss ($L = 1 - R_a - T_a - T_b$, green dash curve) is also plotted to exhibit the evident effect for cavity decays $\gamma_a = \gamma_b = 0.025$. The maximum transfer rate $P_b^{\max}$ also decreases with the increase of the dissipations, as shown in Fig. 5(b), while high transfer rate $P_b^{\max} > 0.9$ is also available for the low dissipations $\gamma_a = \gamma_b = 0.005$ in the common resonator, with $\Omega = 2$ and $g_p = 0.8$. Thus, it is possible to obtain high transfer rate by increasing the coupling strength and the driving to rival the dissipations.

In practice, the waveguide channel length is finite in real experiments. Figure 6 displays the influences of the waveguide length $n\varsigma$ for the maximum transfer rate $P_b^{\max}$, where n is the resonator number, and the lattice constant ς is assumed to be unity. Shown in the figure, $P_b^{\max}$ oscillates remarkably for the front few resonators and smooth gradually with the increasing resonators in the long waveguide channel. The oscillations may arise from the multiple interference of photons located in the supercavity formed by these two atoms.[7] At

$\Omega = 2$ and $g_p = 1.0$, an almost perfect transfer (oscillation peak) without dissipation is achieved for at least four cavities in the right of CRW-a for a bulged waveguide with $N = 4$, while at least six cavities is required to hold a oscillation peak for a bulged waveguide with $N = 6$. $P_b^{\max}$ also reduces slowly for the increase of different dissipations $\gamma_a = \gamma_b = 0.005$ and 0.02. However, for low dissipations $\gamma_a = \gamma_b = 0.005$, high transfer rate $P_b^{\max} = 0.96$ is also obtainable at the 6th cavity in CRW-a for $\Omega = 2$ and $g_p = 1.0$.

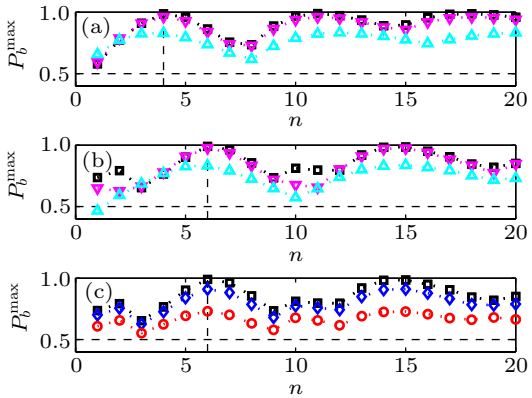


Fig. 6. Maximum transfer rate $P_b^{\max}$ for different resonator number n. (a) Zero dissipation, $\Omega = 2$, $N = 4$, and different coupling g_p: black square curve for $g_p = 1.0$, pink lower triangular curve $g_p = 0.7$, and cyan upper triangular curve for $g_p = 0.35$. (b) Similar to panel (a) except $N = 6$. (c) $\Omega = 2$, $g_p = 1.0$, $N = 6$, and different dissipations: black square curve for zero dissipation, blue diamond curve for $\gamma_a = \gamma_b = 0.005$, and red circle curve for $\gamma_a = \gamma_b = 0.02$. $\gamma_e = \gamma_f = \gamma_{e_2} = 0.001$. The other parameters are the same as those in Fig. 2.

In summary, we investigated the single-photon routing in a T-bulge-shaped waveguide, where a driven Δ-type three-level atom and a two-level atom are embedded in the waveguide resonators. With such an integrated setup, routing properties are discussed in detail for two different photon incident paths. Our results show that bidirectional high transfer-rate quantum routing between different channels can be efficiently performed by adjusting the the resonator-atom coupling and the classical driving, and an additional filtering function generated by the wave interference in the bulged resonators is presented in the scattering spectra. Therefore, this proposed system may be utilized as a highly effective and multi-function quantum router to implement duplex routing.

Appendix A: Scattering amplitudes in the dissipative case

In the appendix, the scattering amplitudes with dissipations in case 1 are calculated, following the similar calculation process in the text. When the dissipations are considered, the corresponding frequencies ω_a, ω_b, ω_e, ω_f, and ω_{e_2} are replaced by ω'_a, ω'_b, ω'_e, ω'_f, and ω'_{e_2}, respectively. Here $\omega'_{a(b,e,f,e_2)} = \omega_{a(b,e,f,e_2)} - \mathrm{i}\gamma_{a(b,e,f,e_2)}$, and $\gamma_{a(b,e,f,e_2)}$ is the decay rate of waviguide-a (b, excited state $|e\rangle$, $|f\rangle$ for the three-level atom, and excited state $|e_2\rangle$ for the two-level atom), respectively. The corresponding effective potentials and the dispersive coupling strength are given by

$$
\begin{aligned}
V'_a(E_k) &= \frac{g_a^2 \Delta'_f}{\Delta'_e \Delta'_f - |\Omega|^2}, \\
V'_b(E_k) &= \frac{g_b^2 \Delta'_e}{\Delta'_e \Delta'_f - |\Omega|^2}, \\
V'_p(E_k) &= \frac{g_p^2}{\Delta'_{e_2}}, \\
G'(E_k) &= \frac{\Omega g_a g_b}{\Delta'_e \Delta'_f - |\Omega|^2},
\end{aligned}
\tag{A1}
$$

with $\Delta'_e = E_k - \omega'_e$, $\Delta'_f = E_k - \omega'_f$, and $\Delta'_{e_2} = E_k - \omega'_{e_2}$.

After some algebra, the revised forms of the scattering amplitudes are expressed as

$$
\begin{aligned}
r_a &= \frac{\xi_a \alpha(0) - \xi_a + \mathrm{i}\gamma_a \mathrm{e}^{-\mathrm{i}k_a}}{\xi_a - \mathrm{i}\gamma_a \mathrm{e}^{\mathrm{i}k_a}}, \\
t_a &= \frac{\xi_a[(\xi_a - \mathrm{i}\gamma_a \mathrm{e}^{-\mathrm{i}k_a})X + (\xi_a - \mathrm{i}\gamma_a \mathrm{e}^{\mathrm{i}k_a})\mathrm{e}^{-2\mathrm{i}pk_a}]\alpha(0)}{[(\xi_a - \mathrm{i}\gamma_a \mathrm{e}^{\mathrm{i}k_a})X + \xi_a - \mathrm{i}\gamma_a \mathrm{e}^{-\mathrm{i}k_a}](\xi_a - \mathrm{i}\gamma_a \mathrm{e}^{\mathrm{i}k_a})}, \\
t_b &= \frac{\xi_b \beta(N)}{(\xi_b - \mathrm{i}\gamma_b \mathrm{e}^{\mathrm{i}k_b})\mathrm{e}^{\mathrm{i}Nk_b}},
\end{aligned}
\tag{A2}
$$

with

$$
\begin{aligned}
\alpha(0) &= \frac{Q_b \xi_a (\mathrm{e}^{\mathrm{i}k_a} \frac{\xi_a - \mathrm{i}\gamma_a \mathrm{e}^{-\mathrm{i}k_a}}{\xi_a - \mathrm{i}\gamma_a \mathrm{e}^{\mathrm{i}k_a}} - \mathrm{e}^{-\mathrm{i}k_a})}{Q_a Q_b - |G'|^2}, \\
\beta(N) &= \frac{G'^* \xi_a (\mathrm{e}^{\mathrm{i}k_a} \frac{\xi_a - \mathrm{i}\gamma_a \mathrm{e}^{-\mathrm{i}k_a}}{\xi_a - \mathrm{i}\gamma_a \mathrm{e}^{\mathrm{i}k_a}} - \mathrm{e}^{-\mathrm{i}k_a})}{Q_a Q_b - |G'|^2}, \\
Q_b &= \mathrm{i}\gamma_b - 2\xi_b \cos k_b + \xi_b \frac{\sin[(N-1)k_b]}{\sin(Nk_b)} \\
&\quad + \frac{\xi_b^2 \mathrm{e}^{\mathrm{i}k_b}}{\xi_b - \mathrm{i}\gamma_b \mathrm{e}^{\mathrm{i}k_b}} - V'_b, \\
Q_a &= \mathrm{i}\gamma_a - 2\xi_a \cos k_a + \frac{\xi_a^2 \mathrm{e}^{\mathrm{i}k_a}}{\xi_a - \mathrm{i}\gamma_a \mathrm{e}^{\mathrm{i}k_a}} \\
&\quad + \frac{\xi_a^2 \mathrm{e}^{\mathrm{i}k_a} X + \xi_a^2 \mathrm{e}^{-\mathrm{i}k_a}}{(\xi_a - \mathrm{i}\gamma_a \mathrm{e}^{\mathrm{i}k_a})X + \xi_a - \mathrm{i}\gamma_a \mathrm{e}^{-\mathrm{i}k_a}} - V'_a, \\
X &= -\frac{[\xi_a \mathrm{e}^{\mathrm{i}k_a} + (\xi_a - \mathrm{i}\gamma_a \mathrm{e}^{\mathrm{i}k_a})Y]\mathrm{e}^{-2\mathrm{i}pk_a}}{\xi_a \mathrm{e}^{-\mathrm{i}k_a} + (\xi_a - \mathrm{i}\gamma_a \mathrm{e}^{-\mathrm{i}k_a})Y}, \\
Y &= \frac{\xi_a \mathrm{e}^{\mathrm{i}k_a}}{\xi_a - \mathrm{i}\gamma_a \mathrm{e}^{\mathrm{i}k_a}} + \frac{\mathrm{i}\gamma_a - 2\xi_a \cos k_a}{\xi_a} - \frac{V'_p}{\xi_a}.
\end{aligned}
\tag{A3}
$$

When the dissipations are not included, the scattering coefficients in Eq. (A2) can be returned to these results in Eq. (11) in the text. While the dissipations are considered, the conservation relation of the photon flow becomes $|t_a|^2 + |r_a|^2 + |t_b|^2 < 1$ due to the leakage.

References

[1] Marcikic I, Riedmatten H D, Tittel W, Zbinden H and Gisin N 2003 *Nature* **421** 509
[2] Shen J T and Fan S 2005 *Opt. Lett.* **30** 2001
[3] Shen J T and Fan S 2005 *Phys. Rev. Lett.* **95** 213001
[4] Chang D E, Sørensen A S, Demler E A and Lukin M D 2007 *Nat. Phys.* **30** 807
[5] Shen J T and Fan S 2009 *Phys. Rev. A* **79** 023837

[6] Zhou L, Gong Z R, Liu Y X, Sun C P and Nori F 2008 *Phys. Rev. Lett.* **101** 100501
[7] Zhou L, Dong H, Sun C P and Nori F 2008 *Phys. Rev. A* **78** 063827
[8] Bernier N R, Tóth L D, Koottandavida A, Ioannou M A, Malz D, Nunnenkamp A, Feofanov A K and Kippenberg T J 2017 *Nat. Commun.* **8** 604
[9] Shen Z, Zhang Y L, Chen Y, Sun F W, Zou X B, Guo G C, Zou C L and Dong C H 2018 *Nat. Commun.* **9** 1797
[10] Maayani S, Dahan R, Kligerman Y, Moses E, Hassan A U, Jing H, Nori F, Christodoulides D N and Carmon T 2018 *Nature* **558** 569
[11] Xia K Y, Nori F and Xiao M 2018 *Phys. Rev. Lett.* **121** 203602
[12] Yang P F, Xia X W, He H, Li S K, Han X, Zhang P, Li G, Zhang P F, Xu J P, Yang Y P and Zhang T C 2019 *Phys. Rev. Lett.* **123** 233604
[13] Zhou L, Yang L P, Li Y and Sun C P 2013 *Phys. Rev. Lett.* **111** 103604
[14] Lu J, Zhou L, Kuang L M and Nori F 2014 *Phys. Rev. A* **89** 013805
[15] Yan W B, Liu B, Zhou L and Fan H 2015 *Europhys. Lett.* **111** 64005
[16] Lu J, Wang Z H and Zhou L 2015 *Opt. Express* **23** 22955
[17] Liu L and Lu J 2017 *Quantum Inf. Process.* **16** 29
[18] Liu L, Yuan J B and Tang S Q 2019 *J. Low Temp. Phys.* **195** 60
[19] Agarwal G S and Huang S 2012 *Phys. Rev. A* **85** 021801
[20] Xia K and Twamley J 2013 *Phys. Rev. X* **3** 031013
[21] Lemr K, Bartkiewicz K, Černoch A and Soubusta J 2013 *Phys. Rev. A* **87** 062333
[22] Yan C H, Wei L F, Jia W Z and Shen J T 2011 *Phys. Rev. A* **84** 045801
[23] Li X M, Xie L Y and Wei L F 2015 *Phys. Rev. A* **92** 063840
[24] Li X M, Xie L Y and Wei L F 2015 *Phys. Rev. A* **92** 063836
[25] Huang J S, Zhang J H, Wang Y and Xu Z H 2018 *Chin. Phys. Lett.* **35** 034201
[26] Huang J S, Wang J W, Wang Y and Li Y L 2019 *Chin. Phys. Lett.* **36** 034202
[27] Aoki T, *et al.* 2009 *Phys. Rev. Lett.* **102** 083601
[28] Hoi I C, *et al.* 2011 *Phys. Rev. Lett.* **107** 073601
[29] Ma X S, Zotter S, Kofler J, Jennewein T and Zeilinger A 2011 *Phys. Rev. A* **83** 043814
[30] Shomroni I, Rosenblum S, Lovsky Y, Brechler O, Guendelman G and Dayan B 2014 *Science* **345** 903
[31] Li Y, Bruder C and Sun C P 2007 *Phys. Rev. Lett.* **99** 130403
[32] Liu Y X, You J Q, Wei L F, Sun C P and Nori F 2005 *Phys. Rev. Lett.* **95** 087001
[33] Blais A, Huang R S, Wallraff A, Girvin S M, Schoelkopf R J 2004 *Phys. Rev. A* **69** 062320
[34] Blais A, Gambetta J, Wallraff A, Schuster D I, Girvin S M, Devoret M H and Schoelkopf R J 2007 *Phys. Rev. A* **75** 032329
[35] Wallraff A, Schuster D I, Blais A, Frunzio L, Majer J, Devoret M H, Girvin S M and Schoelkopf R J 2005 *Phys. Rev. Lett.* **95** 060501